Supporting information

Identification of C_2-C_5 products from CO_2 hydrogenation over PdZn/TiO_2-ZSM-5 hybrid catalysts.

Jonathan Ruiz Esquius[a], Hasliza Bahruji,[b] Michael Bowker[a,c*], Graham J. Hutchings[a*]

* Hutch@cardiff.ac.uk

* BowkerM@cardiff.ac.uk

[a] School of Chemistry, Cardiff Catalysis Institute, Cardiff University, Main Building, Park Place, Cardiff CF10 3AT, UK.

[b] Centre of Advanced Material and Energy Science, University Brunei Darussalam, Jalan Tungku Link, Gadong BE 1410, Brunei Darussalam.

[b] Catalysis Hub, RCAH, Rutherford Appleton Laboratory, Harwell Oxford, Didcot OX11 0QX, UK.

Table of Contents

1. *Commercial ZSM-5 zeolites characterisation*

1.1 Powder X-ray diffraction (XRD) characterisation

ZSM-5 zeolites with different Si:Al ratio (23, 50 and 80) were purchased from Alfa Aesar in their NH_4^+ form. Prior to use or characterisation, the activated H^+-ZSM-5 form was obtained by annealing in static air (550 °C, 10 °C·min^{-1}, 6 h). Obtained XRD patterns (Figure S1) correlated with the MFI morphology of ZSM-5 zeolites (PDF 00-89-1421).

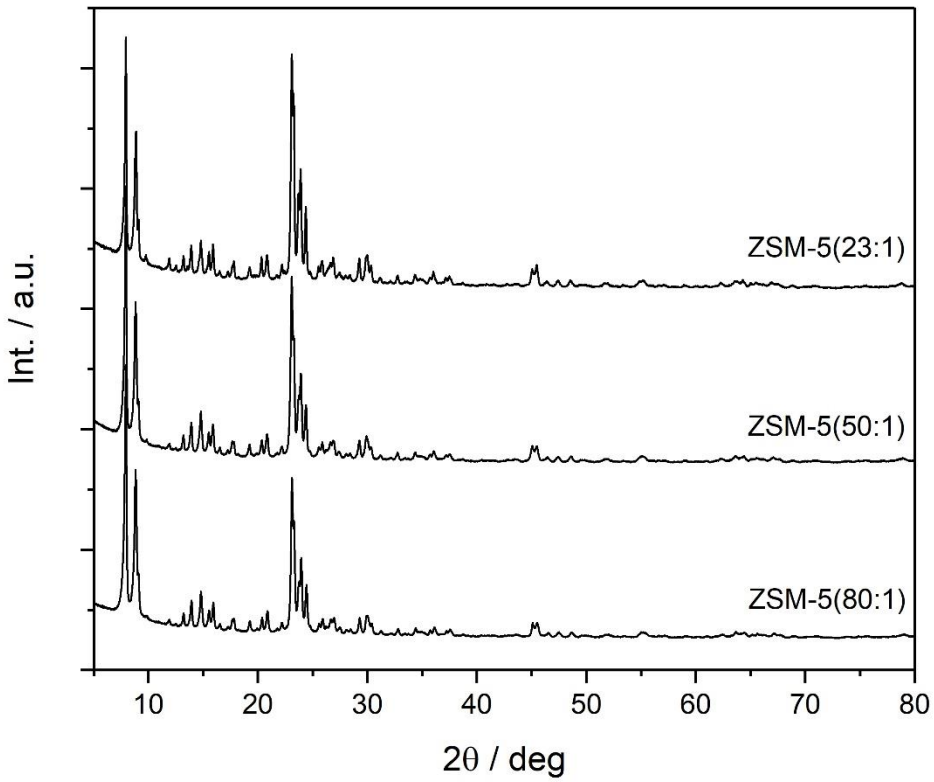

Figure S1. XRD patterns recorded for commercial ZSM-5 zeolites after annealing in static air (550 °C, 10 °C·min^{-1}, 6 h).

1.2 Pore size and BET surface area

Pore size and surface area of annealed ZSM-5 commercial zeolites were obtained from N_2 absorption isotherms at 77 K on a 3-flex micromeritics instrument. Prior to analysis, ZSM-5 zeolites were degassed *in situ* under vacuum at 250 °C for 10 h. A DFT model assuming cylindrical pores and oxide surface was used to obtain the pore size, BET surface areas were obtained on the linear region of the isotherm below at $P/P^0 < 0.3$.[1] As shown in Table S1, no significant changes in pore size neither BET surface area were observed between commercial ZSM-5 zeolites.

Table S1. Pore size and BET surface area obtained from commercial ZSM-5 zeolites after annealing in static air (550 °C, 10 °C·min^{-1}, 6 h) through N_2 absorption.

zeolite	Pore size / Å	BET / m^2 g^{-1}
ZSM-5 (80:1)	5.5 ± 1	461 ± 1
ZSM-5 (50:1)	5.4 ± 1	467 ± 1
ZSM-5 (23:1)	5.3 ± 1	460 ± 1

2. Catalytic activity for CO_2 hydrogenation

The use of PdZn/TiO_2-ZSM-5 hybrid catalysts allow the production of olefins and paraffins directly from CO_2 in a single bed reactor. PdZn/TiO_2 was used as a CH_3OH synthesis catalyst, whilst solid acid ZSM-5 catalysts were used for the consecutive CH_3OH dehydration to DME and the further MTH/DMTH conversion to hydrocarbons.

2.1 CO_2 reaction metrics

PdZn/TiO_2 (0.25 g cat. diluted with 0.25 g of SiC) and PdZn/TiO_2-ZSM-5 hybrid catalysts (0.25 g of methanol synthesis catalyst mixed with 0.25 g of activated zeolite, 425-600 µm pellet size) were tested under CO_2 hydrogenation conditions. The methanol synthesis catalyst consisted of 5 wt.% Pd loading and a Pd to Zn molar ratio of 1:5. Reaction temperature was controlled by placing a thermocouple in the middle of the catalyst bed, catalysts were kept in place using quartz wool. Prior to reaction, catalysts were pre-reduced *in situ* with 5 % H_2/He (400 °C, 5 °C min^{-1}, 1 h). The reactor was then allowed to cool down to 50 °C, the gas flow was swap from 5 % H_2 to the reaction mixture (CO_2/H_2/N_2 = 1/3/1, 30 ml min^{-1}), pressured (20 bar) and heated to the reaction temperature (240, 270, 300, 320, 340 and 360 °C, 5 °C min^{-1}, 6 h dwell at each temperature). Post reaction lines were heated at 120 °C using heating tape to avoid product condensation. Reaction products and reagents were measured online *via* GC analysis fitted with an FID and a TCD detector.

The following calculations were used to determine the CO_2 conversion, product selectivity and productivities:

Through the ideal gas law (equation S1) were P is the pressure of the reaction mixture at the mass flow controller (MFC) (1 bar), R is the gas constant (83.15·10^{-3} dm^3 bar K^{-1} mol^{-1}), T is the temperature (298.15 K) and V is the volume (0.03 dm^3 min^{-1} obtained from the flow gas used during the reaction of 30 ml min^{-1}), the total molar gas (n) flow was determined.

$$PV = nRT \qquad n = 1.21\cdot10^{-3}\ CO_2\ \text{mol min}^{-1} \qquad \text{Eq. S1}$$

Nitrogen gas was used as internal standard at a concentration of 20 vol. %. A blank reactor was analysed simultaneously to the CO_2 hydrogenation reaction, CO_2 conversion was calculated according to equation S2.

$$CO_2 \text{ conv. } \% = \frac{\left(\left(\frac{\text{Blank} \int \text{CO2 / area count}}{\text{Blank} \int \text{N2 / area counts}}\right) - \left(\frac{\int \text{CO2 / area count}}{\int \text{N2 / area counts}}\right)\right)}{\left(\frac{\text{Blank} \int \text{CO2 / area count}}{\text{Blank} \int \text{N2 / area counts}}\right)} \text{ x } 100 \qquad \text{Eq S2}$$

Because the number of moles in the gas phase change during the reaction, a compression factor (CF) was introduced (equation S3).

$$CF = \frac{\int N_2 \text{ / area counts}}{\text{Blank} \int N_2 \text{ / area counts}} \qquad \text{Eq S3}$$

Non-reacted CO_2 was calculated according to equation S4.

$$\text{Non-reacted } CO_2 \text{ mol min}^{-1} = \frac{\frac{\int CO_2 \text{ / area counts}}{rF\ CO_2} \text{ x (total gas flow / mol min}^{-1})}{CF} \qquad \text{Eq S4}$$

CH_3OH productivity was calculated according to equation S5, were *rF* is the response factor obtained from the calibration (area counts per mol^{-1}).

$$CH_3OH \text{ mol min}^{-1} = \frac{\left(\left(\frac{\int CH_3OH \text{ / area counts}}{rF\ CH_3OH}\right) \text{x} \left(\frac{\text{total gas flow/ml min}^{-1}}{\text{0.25 ml loop volume}}\right)\right)}{CF} \qquad \text{Eq S5}$$

Productivity for remaining products was obtained following the next calculations (equation S6 representative for CO productivity), were *rF* is the response factor obtained from the corresponding calibration (area counts per ppm^{-1}).

$$CO \text{ mol min}^{-1} = \frac{\frac{\int CO \text{ / area counts}}{rF\ CO} \text{ x (total gas flow / mol min}^{-1})}{CF} \qquad \text{Eq. S6}$$

The product selectivity based on CO_2 hydrogenation was determined by dividing its productivity times the number of carbons (*nC*) by the productivities of all the products. For instance, methanol and ethane selectivity was calculated following equation S7 and S8, respectively.

$$CH_3OH \text{ sel. } \% = \left(\frac{CH_3OH \text{ productivity x 1C/ mol min}^{-1}}{\Sigma \text{ productivities}}\right) \text{ x } 100 \qquad \text{Eq. S7}$$

$$CH_3CH_3 \text{ sel. } \% = \left(\frac{CH_3CH_3 \text{ productivity x 2C/ mol min}^{-1}}{\Sigma \text{ productivities}}\right) \text{ x } 100 \qquad \text{Eq. S8}$$

Molar productivities obtained in mol min^{-1} could be normalised to the mass of catalysts used during the reaction (0.5 g) and expressed as mol kg_{cat}^{-1} h^{-1} according to equation S9 as shown for methanol.

$$CH_3OH \text{ prod mol } kg_{cat}^{-1}\, h^{-1} = \left(\frac{CH_3OH \text{ productivity / mol min}^{-1}}{(\text{catalyst mass g / 1000})}\right) \text{ x } 60 \qquad \text{Eq. S9}$$

The total CH_3OH productivity, considering that all hydrocarbon except for CO originate from CH_3OH was obtained by adding productivities by the number of carbons (*nC*) as shown in Eq. S10.

$$CH_3OH_{(tot)} \text{ prod mol } kg_{cat}^{-1}\, h^{-1} = \Sigma \text{ prod. x nC} \qquad \text{Eq. S10}$$

Hydrocarbon selectivity based on MTH/DMTH were calculated by diving the individual hydrocarbon productivity multiplied by the number of carbons in the molecule, divided by the total hydrocarbon productivity excluding CH_3OH and DME as shown for ethane in equation S11.

$$CH_3CH_3\ _{(CH3OH)}\text{sel.} = \left(\frac{CH_3CH_3 \text{ productivity x 2C / mol min}^{-1}}{\Sigma \text{ prod. (mol min}^{-1}\text{) x nC}}\right) \qquad \text{Eq. S11}$$

2.2 CO_2 hydrogenation over PdZn/TiO_2

Catalytic data for the CO_2 hydrogenation to CH_3OH for 0.25 g of PdZn/TiO_2 catalyst (diluted with 0.25 g of SiC) is shown in Table S2. Increasing the reaction temperature from 240 to 360 °C resulted in an increase in the CO_2 conversion from 6.8 to 31.2 %. However, in agreement with reaction thermodynamics, CH_3OH selectivity decreases with increasing the reaction temperature, whilst CO formation *via* RWGS is favoured.[2] As observed by the increase in CH_3OH productivity with temperature up to 518 $mmol_{CH3OH}$ kg_{cat} h^{-1} at 300 °C, CH_3OH production below 300 °C occurred in the kinetic regime. At 300 °C, CH_3OH yield (1.27 %) approaches theoretical equilibrium (1.45 %).[2] However, above 300 °C CH_3OH production is limited by thermodynamic equilibrium, as observed by the drop in CH_3OH productivity. DME and CH_4 selectivity remained below 1 % in the temperature range studied.

Table S2. Catalytic data for the CO_2 hydrogenation (20 bar, $CO_2/H_2/N_2$ = 1/3/1, 30 ml·min^{-1}) on 0.25 g $PdZn/TiO_2$ + 0.25 g SiC. Reaction was equilibrated for 6 hours at each temperature. Selectivity are expressed as %, while productivities are in mmol kg_{cat} h^{-1}.

Temp / °C	*X* CO_2 / %	CH_3OH sel. / prod.	DME sel. / prod.	CO sel. / prod.	CH_4 sel. / prod.
240	6.8	24.3 / 340	0.8 / 6	74.6 / 1043	0.3 / 5
270	13.1	15.4 / 486	1.0 / 17	82.6 / 2654	0.5 / 15
300	19.4	9.1 / 518	0.7 / 19	89.6 / 5056	0.6 / 34
320	24.0	4.7 / 333	0.3 / 9	94.4 / 6668	0.6 / 43
340	28.1	2.5 / 207	0.1 / 3	96.7 / 7903	0.7 / 56
360	31.2	1.3 / 115	0.0 / 0	97.9 / 8858	0.8 / 76

2.3 CO_2 hydrogenation over $PdZn/TiO_2$-ZSM-5 hybrid catalysts

$PdZn/TiO_2$-ZSM-5 hybrid catalysts, with Si/Al ratios of 80, 50 and 23 were employed to produce hydrocarbons *via* CO_2 hydrogenation, CH_3OH dehydration to DME and consecutive MTH-DMTH. At the studied temperatures range, no significant differences in the CO_2 conversion or CO productivity were observed for $PdZn/TiO_2$-ZSM-5 hybrid catalysts compared to $PdZn/TiO_2$. Suggesting that CO was produced *via* RGWS over $PdZn/TiO_2$ catalyst, and that the activity of the CH_3OH synthesis catalyst was not altered by the proximity of solid acid ZSM-5 zeolites. To confirm that ZSM-5 is not active to convert CO_2 to either CO or CH_3OH a blank reaction up to 270 °C test was performed on ZSM-5 (23:1). As observed in Table S3, no CO_2 conversion was observed at 240 °C, whilst marginal CO_2 conversion to CO was detected at 270 °C.

Table S3. CO_2 hydrogenation (20 bar, $CO_2/H_2/N_2$ = 1/3/1, 30 ml·min^{-1}) for ZSM-5 (Si/Al = 23/1) (0.5 g, 425 - 625 µm pellet).

Temp / °C	*X* CO_2 / %	CO sel. / %	CH_3OH sel. / %	CH_4 sel. / %
240	n/d	n/d	n/d	n/d
270	0.2	100	0	0

DME was the main oxygenate product on $PdZn/TiO_2$-ZSM-5 hybrid catalysts, indicating that CH_3OH was being effectively dehydrated at solid acid ZSM-5 zeolites. A part of DME, other hydrocarbons product of MTH and DMTH were detected (Table S4). Higher hydrocarbons productivity was observed with increasing the aluminium concentration on ZSM-5 zeolites.

Table S4. Hydrocarbons and oxygenates productivities (mmol kg_{cat} h^{-1}) from $CO_2/H_2/N_2$ = 1/3/1 feed over $PdZn/TiO_2$-ZSM-5 hybrid catalysts (20 bar, 30 ml min^{-1}, 0.5 g_{cat}, 2240-360 °C). The subscript (sat) and = stand for saturated and olefin products: $C_{2(sat)}$, $C_{3(sat)}$, and $C_{4(sat)}$ correspond to ethane, propane and n-butane respectively; c/t C_4 =, c/t C_5 = and n C_5 = correspond to cis/trans-butene, 2-cis/trans-pentene and 1-pentene respectively.

Cat.	Temp / °C	CH_4	C_2 (sat)	C_3 (sat)	CH_3OH	DME	C_4 (sat)	c/t C_4 =	n C_5 =	c/t C_5 =	$C_{(tot)}$
$PdZn/TiO_2$	240	5	-	-	340	6	-	-	-	-	356
	270	15	-	-	486	17	-	-	-	-	535
	300	34	-	-	518	19	-	-	-	-	589
	320	43	-	-	333	9	-	-	-	-	394
	340	46	-	-	207	3	-	-	-	-	270
	360	76	-	-	115	-	-	-	-	-	191
+ZSM5(80:1)	240	11	-	-	61	306	-	-	-	-	691
	270	39	3	-	80	415	-	-	-	-	954
	300	79	36	47	106	110	13	6	10	1	744
	320	95	48	55	104	40	18	8	13	2	714
	340	115	51	21	100	18	5	4	6	1	484
	360	138	53	2	93	8	0.4	-	0.1	-	362
+ZSM5(50:1)	240	12	0.4	-	73	316	-	-	-	-	719
	270	39	5	-	117	420	-	-	-	-	1006
	300	85	38	14	129	117	7	2	3	-	616
	320	95	51	20	117	71	8	2	4	0.2	576
	340	104	62	24	114	36	9	3	6	0.6	566
	360	125	65	7	95	15	2	0.6	1	-	416
+ZSM5(23:1)	240	20	1	-	79	213	-	-	-	-	526
	270	69	26	17	27	288	5	2	4	-	824
	300	139	94	58	32	94	21	7	13	1	904
	320	174	93	45	44	41	15	6	9	1	753
	340	219	86	22	28	16	4	2	3	0.5	559
	360	249	75	12	49	6	1	1	0.6	-	508

Hydrocarbons selectivity was calculated considering that synthesised hydrocarbons originate from MTH and DMTH (Table S5). Note that CH_4 is also produced as by-product from CH_3OH decomposition over TiO_2, since CH_4 was detected for $PdZn/TiO_2$, and hence real selectivity towards CH_4 through MTH and DMTH is lower than reported values. Higher aluminium concentration on the ZSM-5 zeolites resulted in an increase in the selectivity towards higher hydrocarbons.

Table S5. Hydrocarbons selectivity based on MTO and DMTO over $PdZn/TiO_2$-ZSM-5 hybrid catalysts (20 bar, $CO_2/H_2/N_2$ = 1/3/1, 30 ml min^{-1}). $C_{2(sat)}$, $C_{3(sat)}$, and $C_{4(sat)}$ correspond to ethane, propane and n-butane respectively; c/t C_4 =, c/t C_5 = and n C_5 = correspond to cis/trans-butene, 2-cis/trans-pentene and 1-pentene respectively.

$PdZn/TiO_2$	Temp. / °C	CH_4 sel. / %	$C_{2(sat)}$ sel. / %	$C_{3(sat)}$ sel. / %	$C_{4(sat)}$ sel. / %	c/t C_4 = sel. / %	n C_5 = sel. / %	c/t C_5 = sel. / %
+ZSM-5 (80:1)	240	100	0	-	-	-	-	-
	270	87	13		-	-	-	-
	300	24	19	36	15	7	-	-
	320	21	21	37	14	7	-	-
	340	36	32	21	7	4	-	-
	360	55	42	2	1	-	-	-
+ZSM-5 (50:1)	240	88	12	-	-	-	-	-
	270	79	21	-	-	-	-	-
	300	37	31	14	11	2	7	-
	320	31	30	20	12	3	4	-
	340	28	33	19	10	3	8	0.7
	360	42	44	7	3	1	3	-
+ZSM-5 (23:1)	240	89	11	-	-	-	-	-
	270	32	24	23	9	4	9	-

300	20	27	26	12	4	10	0.7
320	28	30	22	9	4	7	0.9
340	44	35	13	3	2	3	0.5
360	56	34	8	1	1	1	-

3. $PdZn/TiO_2$ spent reaction characterisation

3.1 EXAFS fitting parameters for $PdZn/TiO_2$ before and after CO_2 hydrogenation

X-ray absorption spectroscopy (XAS) at Pd K edge was employed to study bulk structural and electronic changes on the PdZn alloy phase after reaction (20 bar, $CO_2/N_2/H_2$ = 1/1/3, 30 $ml \cdot min^{-1}$, 240-360 °C, 6 h dwell, 36 h reaction). Measurements were obtained at B18 Diamond light source at Harwell, Oxford. 100 mg of $PdZn/TiO_2$ after reduction and after reaction were pelleted into an 8 mm diameter disk without diluent. Samples were measured in transmission, a Pd foil was analysed simultaneously and used as a reference. Three scans per sample were averaged before EXAFS analysis, Athena and Artemis software package were used for data interpretation.[3] First and second coordination shell Pd paths were fitted at all *k*-weighted χ data using a *k* space window of 3-12 and a *R* window of 1.15-3.5.

76148 and 09157 crystallographic information files (cif) obtained from the Inorganic Crystal Structure Database (ICSD) were used as references to obtain the respective Pd and PdO crystallographic structures. No suitable cif files of PdZn were obtained to calculate Pd scattering paths. Nevertheless, a suitable PdZn structure was obtained by modifying an isostructural AuCu[4] cif file(reference 180144 from ICSD). Restrictions and parameters employed for EXAFS fitting of the Pd K-edge using Artemis are described in Table S6.

Table S6. Parameters defined and restrictions employed to obtain the coordination number and bond distances for $PdZn/TiO_2$ catalyst after reduction (5% H_2, 400 °C, 5 °C min^{-1}, 1 h) and after reaction (20 bar, $CO_2/H_2/N_2$ = 1/3/1, 240-360 °C, 36 h) using Artemis software. *$Pd_{(a)}$ and $Pd_{(met)}$ corresponds to Pd within the alloy and Pd within metallic palladium respectively. The term "amp" corresponds to the S_0^2 obtained from fitting the palladium foil and was fixed at 0.85.

Path	N / S_0^2	ΔR	σ^2	restrictions
$Pd_{(a)}$-Zn	1 / amp*CN_{Zn}	ΔR_{Zn}	σ^2_{Zn}	CN_{Zn}=14-CN_{Pd1}-CN_{Pd2}
$Pd_{(a)}$-Zn-Pd_1	1 / amp*CN_{Pd1}	ΔR_{Pd1}	σ^2_{Pd1}	CN_{Pd1}=CN_{Pd2}*2
$Pd_{(a)}$-Zn-Pd_2	1 / amp*CN_{Pd2}	ΔR_{Pd2}	σ^2_{Pd2}	
$Pd_{(met)}$-$Pd_{(met)}$	12 / 0.85	$\Delta R_{Pd(met)}$	$\sigma^2_{Pd(met)}$	

3.2 XRD patterns for $PdZn/TiO_2$ before and after CO_2 hydrogenation

EXAFS analysis of $PdZn/TiO_2$ after reduction (400 °C, 5% H_2/Ar, 5 °C·min^{-1}) and after reaction (20 bar, $CO_2/N_2/H_2$ = 1/1/3, 30 ml·min^{-1}, 240-360 °C, 6 h dwell, 36 h reaction) confirmed the stability of the catalytically active PdZn phase (Figure 5). No differences in the first coordination shell (bond distances or coordination number) were observed between catalysts. The presence of metallic Pd and PdZn was detected by EXAFS analysis. In accordance with the PdZn alloy formation mechanism, were the formation of a PdZn layer is formed over a Pd nanoparticle *via* hydrogen spill over.[5,6] The presence of PdZn and Pd after reduction was confirmed by XRD. No changes in peak intensity or broadening on (111) Pd or (111) and (200) PdZn reflection at 40.1°, 41.2° and 44.1° respectively were observed after reaction. The presence of ZnO was also observed at 31.7°, 34.4° and 36.3°. ZnO is formed from the 1:5 excess of $Zn(acac)_2$ to $Pd(acac)_2$ used for the synthesis of the $PdZn/TiO_2$ catalyst. No appreciable differences were observed after reaction on the ZnO reflection. However, a clear intensity rises on rutile TiO_2 and anatase TiO_2 reflections was observed (Figure S2), which could suggest TiO_2 particles agglomeration.

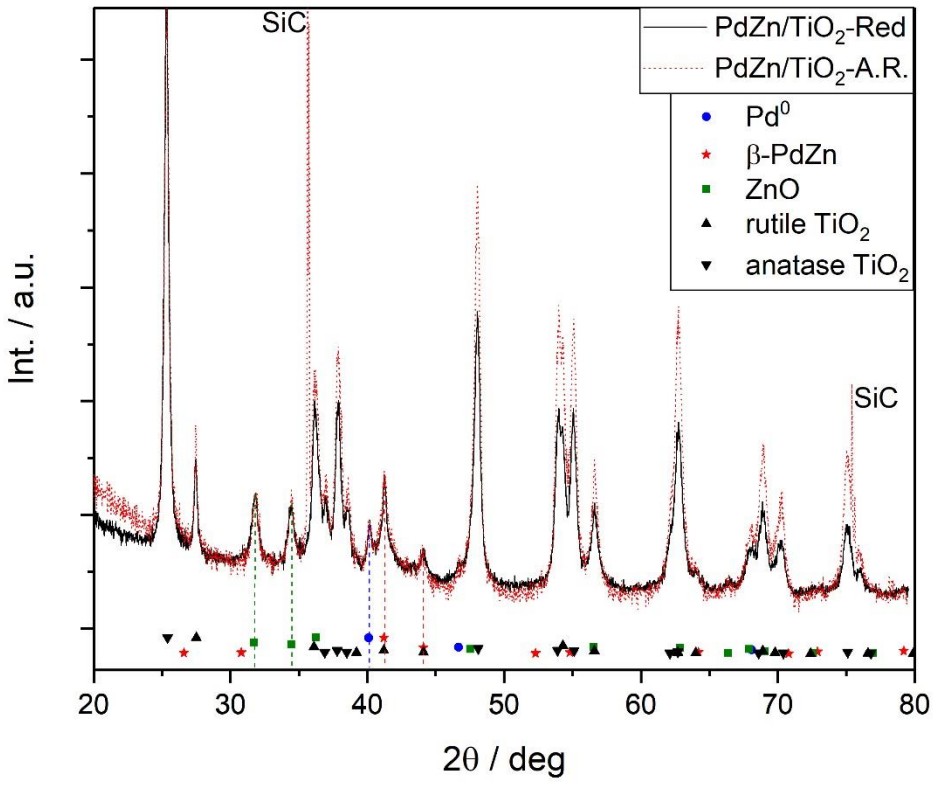

Figure S2. XRD patterns for $PdZn/TiO_2$ recorded after reduction (400 °C, 5 °C min^{-1}, 1 h) and after reaction (20 bar, $CO_2/H_2/N_2$ = 1/3/1, 240 - 360 °C, 36 h).

3.3 XPS characterisation for $PdZn/TiO_2$ before and after CO_2 hydrogenation

To monitor surface changes of the reduced $PdZn/TiO_2$ (400 °C, 5 °C min^{-1}, 1 h) catalyst during reaction (20 bar, $CO_2/H_2/N_2$ = 1/3/1, 240 - 360 °C, 36 h) Pd(3d) and Zn(LM_2) orbitals were analysed by XPS. Due to the low sensitivity towards chemical changes of Zn(2p), Pd(3d) and Zn(LM_2) peaks were calibrated against the Zn(2p) orbital at 1020 eV.[7] The Pd(3d) for $PdZn/TiO_2$ before and after reaction was centred at 335.6 eV, in between reported valued for Pd[8–10] and PdZn.[4,10,11] Peak fitting using Finite-Lorentzian line shapes for Pd and PdZn (including satellites) and Gaussian line shapes for PdO peaks and its satellites with Shirley background[12] confirmed the presence of Pd, PdZn and PdO at 335.0, 335.9 and 337.2 eV respectively (Figure S3a). The Zn(LM_2) main peak for $PdZn/TiO_2$ prior and post reaction was centred 998 eV, a lower in intensity satellite contribution was observed at 991 eV, indicating the presence of ZnO (Figure S3b).

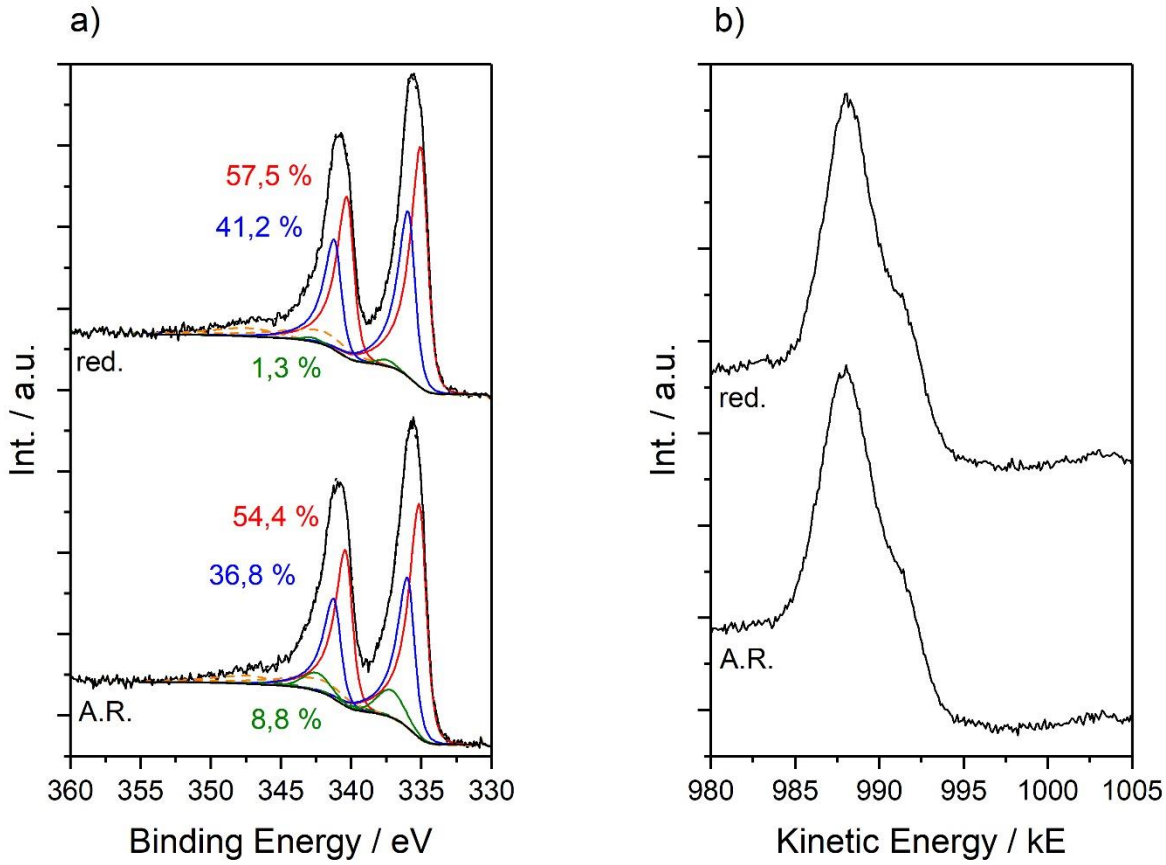

Figure S3. a) Pd(3d) and b) Zn(LM_2) XPS analysis of $PdZn/TiO_2$ catalyst after reduction (red.) in 5% H_2/Ar (400 °C, 5 °C·min^{-1}, 1 h) and after CO_2 hydrogenation (A.R.) (240-360 °C, 36 h, 20 bar, $CO_2/N_2/H_2$ = 1/1/3, 30 ml·min^{-1}). On the Pd(3d) peak, metallic Pd, PdZn and PdO are represented in red, blue and green respectively, Pd and PdZn satellites contributions are represented by an orange dashed line, peak fitting is represented by a dotted line.

3.4 Coke deposition determination by TGA-MS over $PdZn/TiO_2$-ZSM-5 hybrid catalysts during CO_2 hydrogenation

The main deactivation mechanism of zeolites during the conversion of methanol to olefins (MTO) or hydrocarbons (MTH) processes is by coke deposition. Coke can deposit over acid sites, block internal zeolite cavities, and block the zeolite surface limiting CH_3OH diffusion.[13] To determine the extent of coke deposition over $PdZn/TiO_2$-ZSM-5 hybrid catalysts during reaction (240-360 °C, 36 h, 20 bar, $CO_2/N_2/H_2$ = 1/1/3, 30 ml·min^{-1}) fresh and spent samples were analysed by TGA-MS (Figure S4). A steady mass loss was observed under 200 °C which can be attributed to physiosorbed and chemisorbed water. No clear mass loss above 200 °C was detected for $PdZn/TiO_2$-ZSM-5(23) catalyst (Figure S4a). However, a clear 1wt. % mass loss at *c.a.* 200 °C was observed for $PdZn/TiO_2$-ZSM-5(50 and 80) compared to the fresh samples (Figure S4b and S4c, respectively). This loss in weight was accompanied by the release of CO_2 (figure S4e and Figure S4f), the detection of CO_2 at this temperature can be

assigned to coke formation with a high content of oxygen. No coke formation in the form of aromatics was detected at higher temperature.[14]

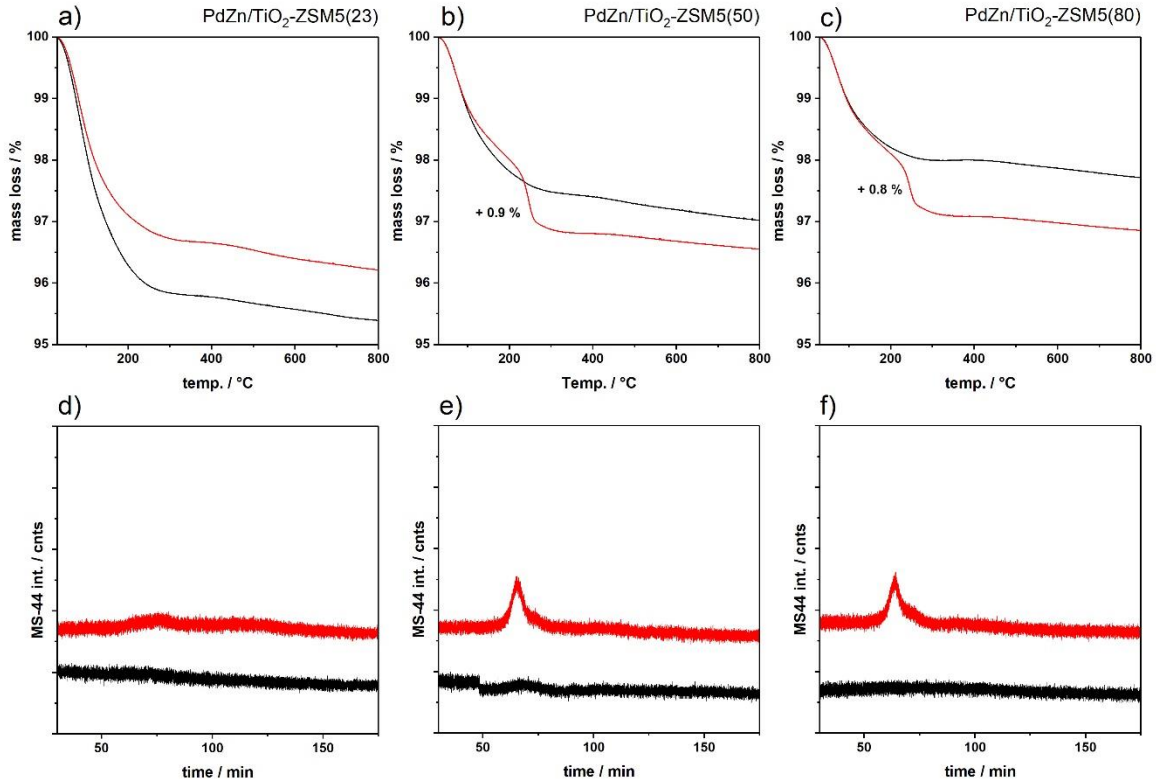

Figure S4. TGA analysis on PdZn/TiO_2-ZSM-5 hybrid catalysts with a Si/Al ratio of a) 23, b) 50 and c) 80 with its respective d), e) and f) mass spectra below. Black and red lines corresponds to fresh and spent (240-360 °C, 36 h, 20 bar, $CO_2/N_2/H_2$ = 1/1/3, 30 ml·min^{-1}) samples, respectively.

References

(1) Sing, K. The Use of Nitrogen Adsorption for the Characterisation of Porous Materials. *Colloids and Surfaces A: Physicochemical and Engineering Aspects* **2001**, *187–188*, 3–9. https://doi.org/10.1016/S0927-7757(01)00612-4.

(2) Shen, W.-J.; Jun, K.-W.; Choi, H.-S.; Lee, K.-W. Thermodynamic Investigation of Methanol and Dimethyl Ether Synthesis from CO2 Hydrogenation. *Korean Journal of Chemical Engineering* **2000**, *17* (2), 210–216. https://doi.org/10.1007/BF02707145.

(3) Ravel, B.; Newville, M. ATHENA, ARTEMIS, HEPHAESTUS: Data Analysis for X-Ray Absorption Spectroscopy Using IFEFFIT. *Journal of Synchrotron Radiation* **2005**, *12* (4), 537–541. https://doi.org/10.1107/S0909049505012719.

(4) Friedrich, M.; Teschner, D.; Knop-Gericke, A.; Armbrüster, M. Influence of Bulk Composition of the Intermetallic Compound ZnPd on Surface Composition and Methanol Steam Reforming Properties. *Journal of Catalysis* **2012**, *285* (1), 41–47. https://doi.org/10.1016/j.jcat.2011.09.013.

(5) Föttinger, K.; van Bokhoven, J. A.; Nachtegaal, M.; Rupprechter, G. Dynamic Structure of a Working Methanol Steam Reforming Catalyst: In Situ Quick-EXAFS on Pd/ZnO Nanoparticles. *J. Phys. Chem. Lett.* **2011**, *2* (5), 428–433. https://doi.org/10.1021/jz101751s.

(6) Penner, S.; Jenewein, B.; Gabasch, H.; Klötzer, B.; Wang, D.; Knop-Gericke, A.; Schlögl, R.; Hayek, K. Growth and Structural Stability of Well-Ordered PdZn Alloy Nanoparticles. *Journal of Catalysis* **2006**, *241* (1), 14–19. https://doi.org/10.1016/j.jcat.2006.04.005.

(7) XPSsimplified.

(8) Brun, M.; Berthet, A.; Bertolini, J. C. XPS, AES and Auger Parameter of Pd and PdO. *Journal of Electron Spectroscopy and Related Phenomena* **1999**, *104* (1), 55–60. https://doi.org/10.1016/S0368-2048(98)00312-0.

(9) Zhang, Y.; Cai, Y.; Guo, Y.; Wang, H.; Wang, L.; Lou, Y.; Guo, Y.; Lu, G.; Wang, Y. The Effects of the Pd Chemical State on the Activity of Pd/Al2O3 Catalysts in CO Oxidation. *Catal. Sci. Technol.* **2014**, *4* (11), 3973–3980. https://doi.org/10.1039/C4CY00552J.

(10) Kast, P.; Friedrich, M.; Girgsdies, F.; Kröhnert, J.; Teschner, D.; Lunkenbein, T.; Behrens, M.; Schlögl, R. Strong Metal-Support Interaction and Alloying in Pd/ZnO Catalysts for CO Oxidation. *Catalysis Today* **2016**, *260*, 21–31. https://doi.org/10.1016/j.cattod.2015.05.021.

(11) Eblagon, K. M.; Concepción, P. H.; Silva, H.; Mendes, A. Ultraselective Low Temperature Steam Reforming of Methanol over PdZn/ZnO Catalysts—Influence of Induced Support Defects on Catalytic Performance. *Applied Catalysis B: Environmental* **2014**, *154–155*, 316–328. https://doi.org/10.1016/j.apcatb.2014.02.032.

(12) Ruiz Esquius, J.; Bahruji, H.; Taylor, S. H.; Bowker, M.; Hutchings, G. J. CO2 Hydrogenation to CH3OH over PdZn Catalysts, with Reduced CH4 Production. *ChemCatChem* **2020**, *12* (n/a). https://doi.org/10.1002/cctc.202000974.

(13) Stöcker, M. Methanol-to-Hydrocarbons: Catalytic Materials and Their Behavior1Dedicated to My Wife Wencke Ophaug.1. *Microporous and Mesoporous Materials* **1999**, *29* (1), 3–48. https://doi.org/10.1016/S1387-1811(98)00319-9.

(14) Janssens, T. V. W. A New Approach to the Modeling of Deactivation in the Conversion of Methanol on Zeolite Catalysts. *Journal of Catalysis* **2009**, *264* (2), 130–137. https://doi.org/10.1016/j.jcat.2009.03.004.